Global and Planetary Change 227 (2023) 104187

Contents lists available at ScienceDirect

Global and Planetary Change

journal homepage: www.elsevier.com/locate/gloplacha

Interannual modulation of the East and South Asian summer precipitation $\delta^{18}O$ by the Indian and western North Pacific summer monsoon strength

Yuanyuan Li [a,b], Xiaodong Liu [a,b,*], Xiaoxun Xie [a], Alexandre Cauquoin [c], Martin Werner [d]

[a] State Key Laboratory of Loess and Quaternary Geology, Institute of Earth Environment, Chinese Academy of Sciences, Xi'an 710061, China
[b] University of Chinese Academy of Sciences, Beijing 100049, China
[c] Institute of Industrial Science, The University of Tokyo, Kashiwa 277-8574, Japan
[d] Alfred Wegener Institute, Helmholtz Centre for Polar and Marine Sciences, Bremerhaven 27570, Germany

ARTICLE INFO

Editor: Dr. Howard Falcon-Lang

Keywords:
Indian summer monsoon
Western North Pacific summer monsoon
Precipitation $\delta^{18}O$
Interannual variability
Walker-type circulation
AGCM

ABSTRACT

The understanding of the relationship between the variation of precipitation stable oxygen isotope ratio ($\delta^{18}O_p$) and monsoon activity in the Asian monsoon region is crucial for an in-depth comprehension of the regional hydrological cycle processes and for reconstructing the history of Asian paleomonsoon changes. Based on the 1979–2017 summer $\delta^{18}O_p$ output by two isotope-enabled atmospheric general circulation models nudged to climate reanalysis data, this study explores the associations of the Indian summer monsoon (IM) and western North Pacific summer monsoon (WNPM) intensities with the interannual variations of the regional $\delta^{18}O_p$ and their possible physical mechanisms. Statistical analyses demonstrate that the East Asian $\delta^{18}O_p$ is negatively correlated with the IM intensity while the Indian $\delta^{18}O_p$ is positively correlated with the WNPM intensity. Moreover, the underlying mechanisms linking the monsoon and $\delta^{18}O_p$ vary in different regions. In strong IM years, with the intensified convection and increased precipitation near the Indian peninsula, the water vapor isotope ratio ($\delta^{18}O_v$) transported to East Asia has lower values, resulting in the depletion of $\delta^{18}O_p$ there. The opposite is true for weak IM years. In years of strong WNPM, the intensified convection over the tropical western Pacific and the suppressed convection over the western Indian Ocean may be linked to a Walker-type circulation anomaly, accompanied by the enlarging of the vertical wind shear between the western Pacific and the western Indian Ocean. Accordingly, the decreasing of convection and precipitation over the Arabian Sea results in higher $\delta^{18}O_v$ values in the upstream area of India, which ultimately increases $\delta^{18}O_p$ values in the Indian peninsula through the monsoonal moisture transport; and vice versa.

1. Introduction

As a natural tracer, the stable oxygen isotope ratio in precipitation ($\delta^{18}O_p$) is widely used for analyzing modern hydrological cycle processes (Gat, 1996; Salamalikis et al., 2016) and reconstructing paleoclimate history (Yang et al., 2016; Ruan et al., 2019). Various observations are used to understand the spatiotemporal characteristics of $\delta^{18}O_p$, such as in situ observations (Hughes and Crawford, 2013; Bedaso et al., 2020) and observation networks (Johnson and Ingram, 2004; Gastmans et al., 2017). In recent years, atmospheric general circulation models equipped with stable water isotopes have been extensively used to explore the spatiotemporal variation of $\delta^{18}O_p$ and its influencing factors, including local and/or regional meteorological elements (Risi et al., 2010; Yang et al., 2017), water vapor transport of oceanic and terrestrial sources (Cole et al., 1999; Li et al., 2016), and upstream rainout effects (Hoffmann and Heimann, 1997; Vuille et al., 2005).

The climate is complex and diverse in Asia, with both monsoon and arid regions where the $\delta^{18}O_p$ variations patterns are distinct and controlled by various factors (Liu et al., 2022). In the Asian inland arid region, the seasonal and interannual variations of $\delta^{18}O_p$ values are usually positively correlated with local air temperature (Wang et al., 2016; Jia et al., 2019), indicating an apparent temperature effect (Dansgaard, 1964). Nonetheless, in the Asian monsoon region (AMR), the $\delta^{18}O_p$ values are mainly low in summer and high in winter (Posmentier et al., 2004; Tian et al., 2021), and primarily dominated by processes related to precipitation formation or water vapor transport

* Corresponding author at: State Key Laboratory of Loess and Quaternary Geology, Institute of Earth Environment, Chinese Academy of Sciences, Xi'an 710061, China.
E-mail address: liuxd@loess.llqg.ac.cn (X. Liu).

https://doi.org/10.1016/j.gloplacha.2023.104187
Received 30 November 2022; Received in revised form 25 June 2023; Accepted 5 July 2023
Available online 10 July 2023

(Cai and Tian, 2016a), yet the specific physical mechanisms are complicated. This paper focuses on the June–July–August (JJA) $\delta^{18}O_p$ variability in the AMR, where precipitation appears mainly in summer and the summer $\delta^{18}O_p$ is the main contributor of the annual mean signal.

To explain the controlling factors of AMR $\delta^{18}O_p$, previous studies focused on the amount effect—the inverse correlation between $\delta^{18}O_p$ and rainfall (Dansgaard, 1964; Araguás-Araguás et al., 1998; Liu et al., 2008). However, recent studies have suggested that the effects of upstream large-scale atmospheric processes are more profound, especially the upstream convection and rainout that deplete downstream $\delta^{18}O_p$ (Midhun and Ramesh, 2016; Yang et al., 2016; Zhou et al., 2019). The strong interannual variation of AMR $\delta^{18}O_p$ and its connection with the atmospheric circulation patterns regulated by the El Niño–Southern Oscillation (ENSO) phenomenon have attracted much attention. As a coupled oscillation in the tropical Pacific Ocean and atmosphere, ENSO significantly affects the Asian monsoons by modulating the Walker circulation (Webster and Yang, 1992; Lau and Nath, 2003). It has been proposed that ENSO could influence AMR $\delta^{18}O_p$ by adjusting the relative contributions of water vapor from different source regions (Tan, 2014; Zhou and Li, 2018), the convective activities in moisture source regions (Ruan et al., 2019) or the distillation processes during the transport (Ishizaki et al., 2012). Some studies have explored the link between the Asian monsoon circulation and $\delta^{18}O_p$. For example, from the perspective of intra-seasonal and seasonal changes, there are significant $\delta^{18}O_p$ variations when the summer monsoon is established (Yang et al., 2012; Yu et al., 2016). However, the interpretation of the interannual $\delta^{18}O_p$ variation in the AMR remains controversial. Some studies indicated that the $\delta^{18}O_p$ signals respond to the monsoon activity that changes the contribution of water vapor sources (Tang et al., 2017; Kathayat et al., 2021). Several investigators showed that the change of upstream precipitation (Yang et al., 2016; Wang et al., 2020) could be transmitted to downstream $\delta^{18}O_p$ variations. Also, Tan (2014) suggested that the $\delta^{18}O_p$ variations might reflect the relative contributions of different monsoon subsystems modulated by ENSO. During El Niño (La Niña) events, the enhanced southeast (southwest) monsoon promotes (restrains) the long-distance transportation of water vapor and leads to more negative (positive) $\delta^{18}O_p$ values (Tan, 2014).

The Asian summer monsoon consists of three relatively independent and interactive subsystems: the tropical Indian summer monsoon (IM), the tropical western North Pacific summer monsoon (WNPM) and the subtropical East Asian summer monsoon (EAM) (Murakami and Matsumoto, 1994; Wang and LinHo, 2002). Among them, the IM and the WNPM correspond to the continental monsoon system and the oceanic monsoon system, respectively (Wang and LinHo, 2002). The changes in the intensity of these two monsoon systems have diverse impacts on the regional climate (Wang et al., 2001). During strong IM, precipitation increases from India to the Bay of Bengal; while during strong WNPM, precipitation increases in the South China Sea and the Western Pacific. The EAM is regulated by these two tropical monsoon sub-systems to a certain degree, and the WNPM has a more profound impact on the EAM than the IM. Therefore, the WNPM index with a reversed sign can be used to represent the EAM intensity (Wang et al., 2008). Although the AMR $\delta^{18}O_p$ has been shown to have relations with the monsoon circulation and its associated moisture transport, comparative researches involving the effects of these monsoon subsystems on $\delta^{18}O_p$ in various regions are still rare. In this study, we utilize the simulation results from two isotope-enabled atmospheric general circulation models (AGCMs) to explore the regional differences in the associations of the IM and WNPM intensities with the interannual variations of $\delta^{18}O_p$ and their physical mechanisms.

2. Materials and methods

2.1. Study area

This study mainly focuses on the Asian monsoon area where the climate is controlled by tropical and subtropical monsoons. Two specific regions are selected as representatives of tropical IM (75°–80°E and 13°–20°N) and subtropical EAM (105°–115°E and 25°–35°N) (see below for details), with strong seasonality of precipitation (i.e., wet summers and dry winters). These areas receive abundant moisture during the summer monsoon season from the Indian Ocean, the Bay of Bengal, the South China Sea and the western North Pacific (Wang and LinHo, 2002). In addition, the $\delta^{18}O_p$ values are very distinct seasonally and spatially in different parts of Asia (Liu et al., 2022). For example, summer $\delta^{18}O_p$ values in South Asia are generally higher than those in East Asia.

2.2. Simulated $\delta^{18}O_p$ and $\delta^{18}O_v$

In this study, the monthly $\delta^{18}O_p$ and $\delta^{18}O_v$ values for the period 1979–2017 were taken from the outputs of two AGCMs, ECHAM6-wiso and isoGSM2, in order to take into account possible model dependence of the simulation results and to confirm the robustness of our analysis results. ECHAM6 is the sixth-generation atmospheric circulation model developed by the Max Planck Institute for Meteorology (Stevens et al., 2013) and its isotope-enabled version is called ECHAM6-wiso (Cauquoin et al., 2019). The temperature, vorticity, divergence and logarithm of surface pressure fields have been nudged to the 6-hourly ERA5 meteorological data, provided by the ECWMF (Hersbach et al., 2020). The sea surface temperature (SST) and sea ice area fraction fields from ERA5 have been used as sea surface boundary conditions for the model. Since the model spatial resolution has a significant impact on the regional-scale simulation (Werner et al., 2011), a relatively high resolution (T127L95, ~0.9° × 0.9° horizontal resolution and 95 vertical levels) with better simulation performance was selected. A detailed description of the ECHAM6-wiso model and the simulation experiments that we used in this study can be found in Cauquoin and Werner (2021).

The isoGSM2 is the second-generation Global Spectral Model incorporating isotopic processes developed by the Scripps Experimental Climate Prediction Center (Yoshimura et al., 2008). SST and sea ice area fractions from the National Center for Environmental Prediction (NCEP) reanalysis 2 (Kanamitsu et al., 2002) have been used as boundary conditions. The model has been nudged to the 6-hourly NCEP2 meteorological data (Chiang et al., 2020), including temperature, zonal and meridional winds. It has a horizontal resolution of T62 (~200 km) and 28 vertical layers. Further information on the isoGSM2 model and the simulation experiments can be found in Yoshimura et al. (2008) and Chiang et al. (2020). The simulated isotope values constrained by the observed atmospheric fields are in good agreement with the isotopic observations (Yoshimura et al., 2008; Risi et al., 2010; Yang et al., 2016), and bring an important added value for understanding the spatiotemporal variation characteristics of $\delta^{18}O_p$ (Yoshimura et al., 2008).

2.3. Climate data

In the following, we used meridional and zonal wind fields, air temperature and relative humidity from NCEP/DOE reanalysis data (Kanamitsu et al., 2002), as well as calculated vertically integrated moisture flux (1000 hPa–300 hPa, same below). Global precipitation data were obtained from the CPC Merged Analysis of Precipitation (CMAP) (Xie and Arkin, 1997). Besides, we also used outgoing longwave radiation (OLR) data provided by NOAA satellites (Liebmann and Smith, 1996). The OLR reflects the strength of convective activity (Wang and Xu, 1997) by measuring the cloud-top temperature. The lower (higher) the cloud-top temperature, the stronger (weaker) the convective activity. The above data are monthly values during 1979–2017 with a horizontal resolution of 2.5° × 2.5°.

2.4. Data processing and statistical methods

The monsoon intensity is generally reflected by the monsoon index. We calculated the Indian Monsoon Index (IMI) and the western North

Pacific Monsoon Index (WNPMI) for each year in the period 1979–2017 using the NCEP/DOE reanalysis data, as in Wang et al. (2001). The IMI is defined as the difference of 850 hPa zonal winds between 5°–15°N, 40°–80°E and 20°–30°N, 70°–90°E in summer. The WNPMI is defined as the difference of 850 hPa zonal winds between 5°–15°N, 100°–130°E and 20°–30°N, 110°–140°E in summer. The larger the monsoon index, the stronger the monsoon intensity. The definitions of these indexes have been widely used to investigate the time variations of the Asian regional monsoons and their mechanisms (Wang et al., 2001; Terray et al., 2003; Yim et al., 2008; Sheng et al., 2022). It should be noted that the monsoon index series calculated with the NCEP/DOE data are highly correlated with those calculated using the ERA5 reanalysis data or the corresponding simulated data from ECHAM6-wiso or isoGSM2 (see Fig. S1, Tables S1 and S2 of the supplementary material).

In this paper, the monthly values weighted by the monthly precipitation rates were used to calculate the summer $\delta^{18}O_p$ values (e.g., Rozanski et al., 1993). The linear relationships between $\delta^{18}O_p$ and climate variables were evaluated by the Pearson correlation coefficient and tested for significance by Student's t-distribution (Wilks, 2019). The responses of climate variables to monsoon intensities were assessed by unary linear regression, and the corresponding regression coefficients were calculated by the least squares method (Wilks, 2019) and tested for significance by Student's t-distribution.

3. Results and discussion

3.1. Distribution of Asian summer $\delta^{18}O_p$ and its correlation with regional monsoon intensity

To understand the variation of summer $\delta^{18}O_p$, we first analyzed its spatial distribution in Asia and the Indo-Pacific region (Fig. 1). Both model results show similar spatial patterns and some common characteristics. (1) The $\delta^{18}O_p$ values are more positive in the tropical Indian Ocean than in the western Pacific warm pool, due to different oceanic evaporative source regions (Gimeno et al., 2012; Castillo et al., 2014) and to strong convection over the western Pacific warm pool that amplifies the amount effect (Sutanto et al., 2015). (2) Relatively low $\delta^{18}O_p$ values are modeled over the Tibetan Plateau, due to a combination of the altitude and continental effects (Araguás-Araguás et al., 2000). (3) The $\delta^{18}O_p$ values are more negative in East Asia and less negative in South Asia. The isotopic content of precipitation in these areas is affected by moisture sources, moisture transport paths, and atmospheric circulation patterns (Tan, 2014; Cai and Tian, 2016b; Midhun et al., 2018; Rahul and Ghosh, 2019).

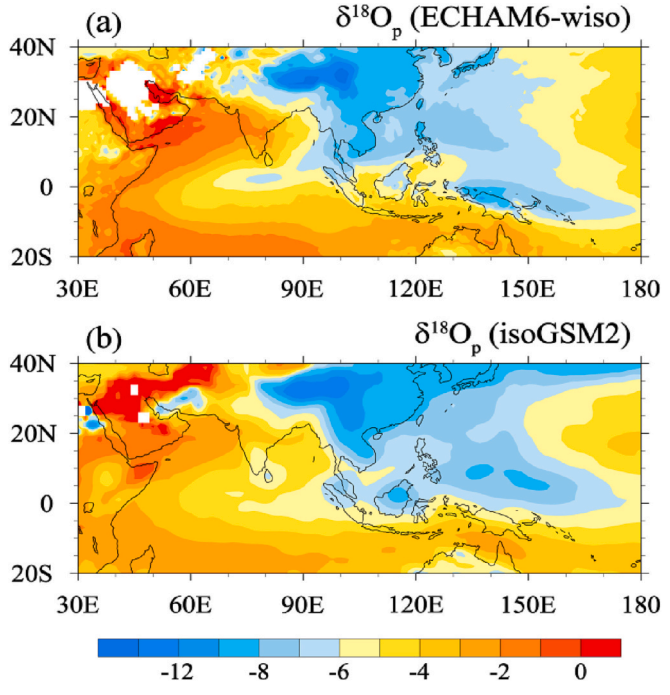

Fig. 1. Spatial distribution of summer-averaged $\delta^{18}O_p$ over the Asia and tropical Indo-Pacific region from 1979 to 2017 simulated by (a) ECHAM6-wiso and (b) isoGSM2.

We noticed differences in the modeled $\delta^{18}O$ values between the two model simulations, too. For example, the values of ECHAM6-wiso are higher by ~1.67 and lower by ~0.57 than those of isoGSM2 from the Arabian Sea to India and in the Tibetan Plateau, respectively. This is possibly due to the differences in the driving fields and physical parameterizations of the models, including the spatial resolution. The overall $\delta^{18}O_p$ distribution characteristics are consistent with those of June–September $\delta^{18}O_p$ simulated by the SWING2 models in Midhun and Ramesh (2016).

Then, we examined the responses of $\delta^{18}O_p$ to different Asian monsoon subsystems (Fig. 2). As shown in Fig. 2a and b, the correlation distributions between the IMI and $\delta^{18}O_p$ exhibit similar characteristics for the two AGCMs, with significant negative correlations from the Bay of Bengal to Indochina and extending to East Asia ($r = -0.4$ to $-0.6, p < 0.01$). That is, the stronger the IM, the more depleted the $\delta^{18}O_p$ values are. This is in agreement with Wang et al. (2020) who also found a negative correlation between local $\delta^{18}O_p$ and the IM intensity through a fixed-point observation study in eastern China. Since our study focuses on the $\delta^{18}O_p$ variations in the monsoon region on land, the area with high negative correlations (105°–115°E; 25°–35°N; red box in Fig. 2a and b) was selected as the EAM representative area (abbreviated as EA below).

For the WNPMI, the correlation coefficients with $\delta^{18}O_p$ (Fig. 2c and d) are generally similar regardless the model used. We find positive correlation coefficients in the Indian Ocean and from the Indian Peninsula to western Maritime Continent ($r = 0.4$ to $0.8, p < 0.01$), and negative correlations in the tropical western Pacific ($r = -0.4$ to -0.6, $p < 0.01$). During strong WNPM, $\delta^{18}O_p$ is enriched over the Indian Ocean and depleted over the Western Pacific warm pool, and vice versa. Previous observational studies also revealed that the $\delta^{18}O_p$ signals in the western Pacific stations are negatively correlated with rainfall (Araguás-Araguás et al., 1998). Because the precipitation rates increase in the western North Pacific when the WNPM intensifies, this reflects the relationship between $\delta^{18}O_p$ in the tropical western Pacific and WNPM, supporting our conclusion. Similar to EA, we chose the area with high positive correlations on land (75°–80°E; 13°–20°N; blue box in Fig. 2c and d) as the IM representative area (hereinafter referred to as ID).

To evaluate the interannual relationships between $\delta^{18}O_p$ and monsoon intensities in different monsoon regions, we compared the time series of two model-averaged EA (ID) $\delta^{18}O_p$ and the IMI (WNPMI). During our period of interest, the two monsoon indices and the regional-averaged $\delta^{18}O_p$ of the representative area show prominent interannual variations (Fig. 3). The IMI is negatively correlated with EA $\delta^{18}O_p$ ($r = -0.55$, $p < 0.01$; Fig. 3a) while the WNPMI is positively correlated with ID $\delta^{18}O_p$ ($r = 0.62$, $p < 0.01$; Fig. 3b). The IMI (WNPMI) monsoon index series have similar correlations with the EA (ID) $\delta^{18}O_p$ series from each individual model (not shown). The robustness of the monsoon–$\delta^{18}O_p$ relationships has been tested by calculating the correlations between differently defined monsoon indices and $\delta^{18}O_p$ (not shown). In the following, we will further investigate the link between the IM (WNPM) intensity and EA (ID) $\delta^{18}O_p$ changes.

3.2. Effect of the IM intensity on the East Asian $\delta^{18}O_p$ and its mechanism

In this section, we analyzed the high temporal correlation between the IMI and EA $\delta^{18}O_p$ variations and the underlying physical processes. The regional precipitation and convection are closely associated with the IM intensity, as shown in Fig. 4. When the IM strengthens, precipitation (Fig. 4a) and convection (Fig. 4b) are increased from the Indian

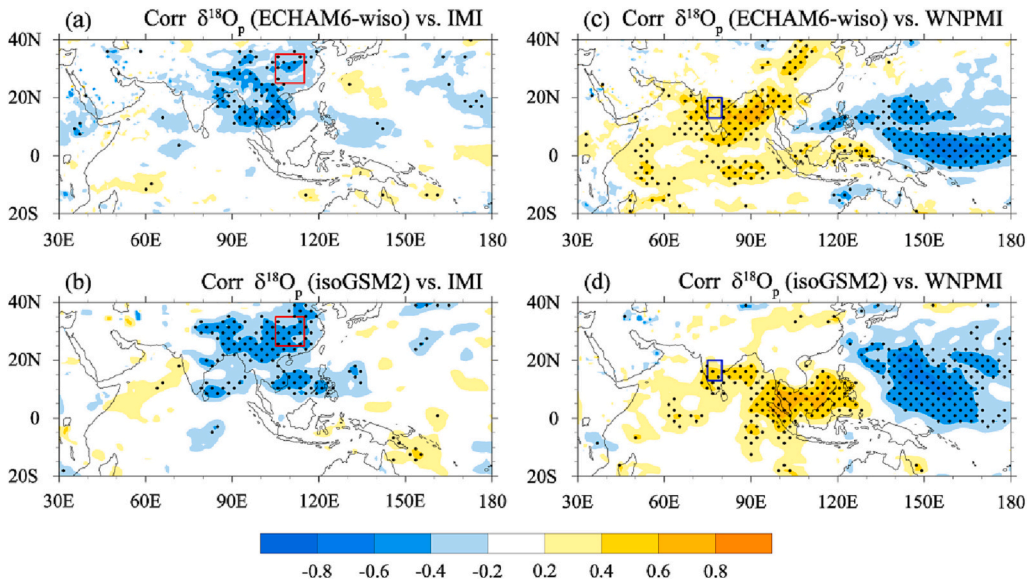

Fig. 2. Spatial distribution of correlation coefficients between IMI and $\delta^{18}O_p$ simulated by (a) ECHAM6-wiso and (b) isoGSM2 in the Asia and Indo-Pacific region from 1979 to 2017; (c) and (d) are same as (a) and (b), respectively, but for correlation coefficients between WNPMI and $\delta^{18}O_p$. The black dots represent values exceeding the 95% confidence level. The red and blue rectangles indicate the EA and ID, respectively. (For interpretation of the references to colour in this figure legend, the reader is referred to the web version of this article.)

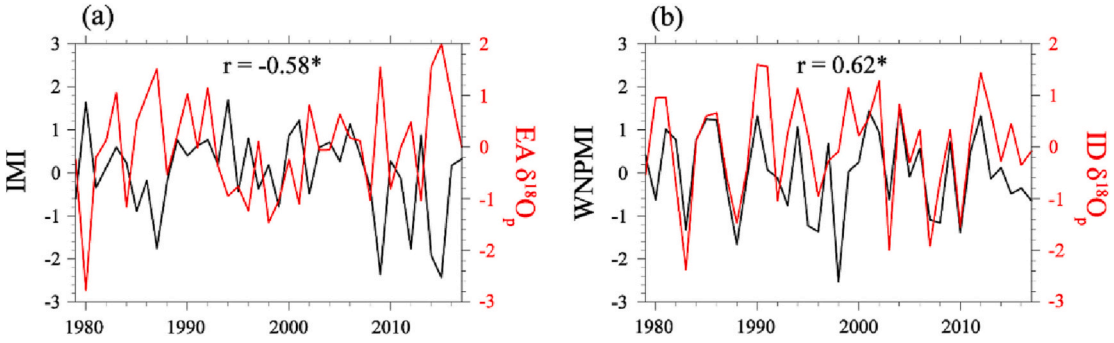

Fig. 3. (a) Normalized time series of summer-averaged IMI and two model-averaged EA $\delta^{18}O_p$ from 1979 to 2017, (b) Same as (a), but for WNPMI and ID $\delta^{18}O_p$. The "r" is the correlation coefficient between the two series, and the "*" means exceeding the 99% confidence level.

peninsula to the Bay of Bengal. The areas with high correlation in Fig. 4a and b are consistent with each other, namely the intensification of convection in South Asia corresponds to the increase in precipitation (Prasad and Bansod, 2000). On the other hand, we noticed that the IM does not affect the precipitation or convection in East Asia, since there is no significant correlation in the red box in Fig. 4. Therefore, the $\delta^{18}O_p$ changes of EA do not respond directly to the variations of IM intensity through the amount effect.

To understand how the IM-induced precipitation and convection anomalies in upstream South Asia (Fig. 4) affect the $\delta^{18}O_p$ variations in downstream East Asia (Fig. 2a and b), we conducted a correlation analysis of the IMI with modeled $\delta^{18}O_v$ and a regression analysis with the vertically integrated moisture flux (Q flux) (Fig. 5). We found that the IMI is negatively correlated with EA and its upstream $\delta^{18}O_v$ (Fig. 5a and b) in both models. The source of moisture for the EA comes mainly from South Asia. It is the upstream $\delta^{18}O_v$ depletion that leads to $\delta^{18}O_v$ depletion in the EA through monsoon advection during periods of enhanced IM. However, our regression analysis indicates that the moisture transport from South Asia to East Asia is reduced in response to the enhanced IM (Fig. 5c). Therefore, the $\delta^{18}O_p$ depletion of EA mainly depends on changes in $\delta^{18}O_v$ caused by upstream convection and precipitation rather than moisture transport. Previous studies have also indicated that this upstream effect can alter $\delta^{18}O_p$ in East Asia (Lee et al., 2012; Wang et al., 2020). Furthermore, an isotopic study of the simulated Heinrich event influencing the Asian paleoclimate also supports this explanation (Pausata et al., 2011).

3.3. Association of WNPM intensity with south Asian $\delta^{18}O_p$ and its mechanism

In Section 3.1 we have shown that the WNPMI is strongly correlated with the ID $\delta^{18}O_p$. We analyze here the mechanisms underlying this correlation. The correlation between the WNPMI and rainfall is positive in the western Pacific warm pool and negative from the Arabian Sea to the Maritime Continent (Fig. 6a), which is opposite to the correlation between WNPMI and convection (Fig. 6b). Although the WNPMI may have a weak correlation with ID precipitation (blue box in Fig. 6a), the South Asian $\delta^{18}O_p$ is only partly modulated by local precipitation (Ishizaki et al., 2012; Midhun and Ramesh, 2016). Therefore, the link between the WNPMI and ID $\delta^{18}O_p$ (as shown in Figs. 2c-d and 3b) should depend on other physical processes.

We analyzed the physical processes behind the ID $\delta^{18}O_p$ change associated with the WNPM in Fig. 7. The correlation fields between the WNPMI and $\delta^{18}O_v$ (Fig. 7a and b) indicate that changes in WNPM and variations in $\delta^{18}O_v$ are closely related on a wide spatial range, with negative and positive correlations over the western Pacific warm pool and the Indian Ocean, respectively. The latter covers the main moisture source areas of the IM precipitation (Pathak et al., 2017). There is no increase in northward moisture transport over the western Indian Ocean as the WNPM strengthens (Fig. 7c), which means that the changes in ID $\delta^{18}O_p$ cannot be attributed to those in the moisture transport. The significant positive correlations of WNPMI with rainfall and convection in the Arabian Sea upstream of the ID (Fig. 6a and b) suggest that the

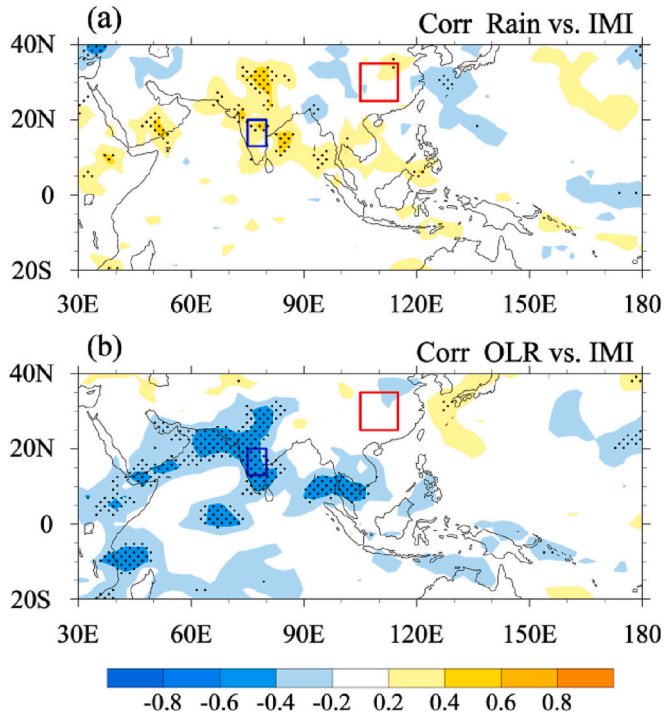

Fig. 4. Distributions of correlation coefficients between IMI and (a) summer rainfall as well as (b) summer OLR during 1979–2017. The black dots represent values exceeding the 95% confidence level.

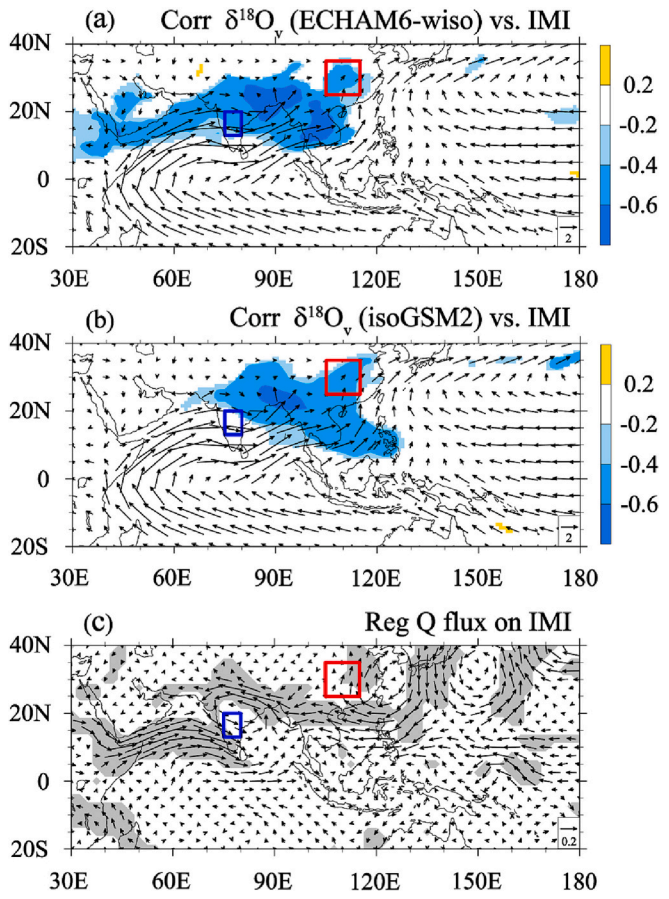

Fig. 5. Spatial distribution of correlation coefficients between IMI and $\delta^{18}O_v$ simulated by (a) ECHAM6-wiso and (b) isoGSM2 throughout the Asian and Indo-Pacific region during the period 1979–2017 (shaded, only correlation coefficients above the 95% confidence level are shown) and vertically integrated climatological summer moisture flux (vector, 10^2 kg m^{-1} s^{-1}); (c) The summer vertically integrated moisture flux (10^2 kg m^{-1} s^{-1}) regressed against IMI during 1979–2017, the shading represents values exceeding the 95% confidence level.

rainout processes in the Arabian Sea related to changes in WNPM are the direct cause of the variations in ID $\delta^{18}O_p$.

Next, we discuss how the precipitation and convection in the Arabian Sea are associated with the WNPM. The western Pacific warm pool is one of the regions with the highest sea surface temperature and most active convection in the world, and plays a major role in driving tropical circulation anomalies (Webster, 1994). Previous studies have shown that the WNPM is closely connected with convective activity over the western Pacific warm pool (Wang et al., 2022). A strong (weak) WNPM is usually accompanied by an anomalous cyclonic (anticyclonic) circulation over the western North Pacific (Wu et al., 2009), corresponding to an intensification (a suppression) of the convection in the western Pacific warm pool (Wang et al., 2013). To examine the link between convection and the WNPM in the Indo-Pacific, we performed a linear regression analysis of OLR versus the WNPMI (Fig. 8a), representing the OLR mean change in response to the WNPM intensity. For example, a regression coefficient of +2.0 corresponds to an increase of 2 W/m^2 in OLR for one unit increase of the WNPMI value. The results show that the convective activities in the Pacific warm pool and the Arabian Sea–-tropical Indian Ocean are distinct and present opposite changes relative to WNPM variations. The convective activities are enhanced (reduced) in the Pacific warm pool and reduced (enhanced) in the Arabian Sea–-tropical Indian Ocean region under strong (weak) WNPM conditions. Using the differences in OLR (denoted as ΔOLR) between the western Pacific warm pool (orange box in Fig. 8a, 62°–72°E; 10°–15°N) and the Arabian Sea (green box, 130°–145°E; 10°–15°N) to reflect the intensity of see-saw changes in east-west convective activity, we can see that the interannual variations of the WNPMI and ΔOLR are highly correlated (Fig. 8b). This may be the role of the zonal Walker-type circulation in the equatorial Indian Ocean (Hastenrath, 2000; Pohl and Camberlin, 2011) or the tropical Pacific–Indian Ocean (Li and Zhou, 2014).

According to previous studies, the zonal circulations in the upper (150 hPa) and lower (850 hPa) atmosphere pressure levels over the tropical Indian Ocean have reverse signals (Pohl and Camberlin, 2011). In the climatological wind fields (Fig. 8c), the westerly and easterly winds prevail at the upper and lower levels in the tropical Indian Ocean (purple box, 70°–130°E; 10°–15°N), respectively. Hence, referring to Pohl and Camberlin (2011), we constructed a zonal wind (the "U" component, i.e., the east-west component of the wind vector) shear index (abbreviated as USI) based on the difference between the normalized zonal winds of the upper and lower levels averaged in this region. The higher the USI, the greater the zonal wind shear over the tropical Indian Ocean. The time series in Fig. 8d indicate that the WNPM intensity is highly negatively correlated with the zonal circulation changes over the Indian Ocean. Overall, in years of strong WNPM, the upward motion of the Pacific warm pool and the simultaneous subsidence over the Arabian Sea are relatively strong, resulting in a stronger easterly (westerly) wind anomaly at the upper (lower) level of the tropical Indian Ocean and, correspondingly, a strengthening of the Walker-type zonal circulation; and vice versa. Thus, the Walker-type circulation changes synchronously with the WNPM intensity and links the convective activities over the Pacific warm pool and the Arabian Sea. It influences the precipitation rates and $\delta^{18}O_v$ values upstream of the Indian peninsula, which ultimately leads to a change of $\delta^{18}O_p$ in ID.

This tentative explanation needs further verification, and the mechanisms linking convection over the Pacific warm pool to the $\delta^{18}O_v$ over the Arabian Sea also merit further investigation in the future. For example, it is possible that convection anomalies over the Arabian Sea and the Pacific warm pool are jointly influenced by a large-scale

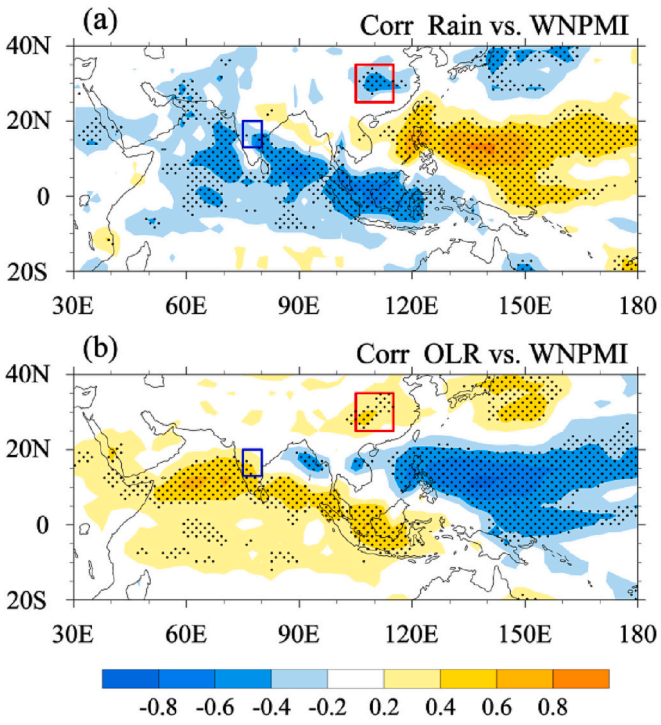

Fig. 6. Same as Fig. 4, but for WNPMI.

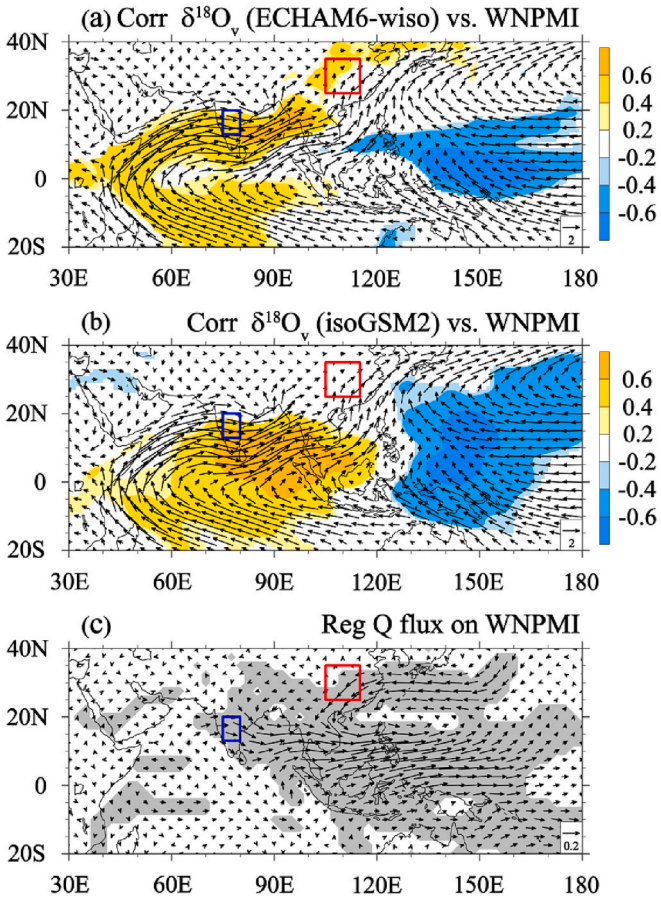

Fig. 7. Same as Fig. 5, but for WNPMI.

circulation, although there is evidence to suggest that the anomaly of the tropical mid-eastern Pacific Ocean SST precedes the tropical Indian SST anomaly by 3 months through the Asian monsoon circulation and the Walker circulation (Feng et al., 2012). Anyway, the relationship between the interannual variations in convective activities over the tropical western Pacific and western Indian Oceans remains to be clarified.

4. Conclusions

Based on statistical analyses of modeled 1979–2017 summer $\delta^{18}O_p$ values from nudged ECHAM6-wiso and isoGSM2 simulations as well as NCEP/DOE reanalysis data, we investigated the modulations of the IM and WNPM intensities on the interannual variations of the Asian summer $\delta^{18}O_p$ and the underlying mechanisms. We found that the EA $\delta^{18}O_p$ was negatively correlated with the IMI while the ID $\delta^{18}O_p$ was positively correlated with the WNPMI. Further analyses indicate that EA $\delta^{18}O_p$ responds to the IM mainly through the upstream depletion effect. We also suggest that the concomitant variations in ID $\delta^{18}O_p$ and WNPM, attributed to the anomalous convective activities over the Arabian Sea and the Pacific warm pool, may be linked to a Walker-type circulation anomaly over the tropical western Pacific–Indian Ocean.

We summarized our findings in the schematic diagram in Fig. 9. When the IM strengthens, convection and precipitation processes near the Indian Peninsula increase, leading to a depletion of the upstream $\delta^{18}O_v$. The latter is transported to East Asia by the monsoon airflow and results in depleted $\delta^{18}O_p$ values (Fig. 9a), and vice versa (Fig. 9b). There is a close association between the WNPM and the convection intensity over the western Pacific warm pool. When the WNPM strengthens (an anomalous cyclone occurs in the western North Pacific), the anomalous airflows converge and rise over the Pacific warm pool, but sink and diverge over the western Indian Ocean, promoting tropospheric wind shear across the two regions. That is, a Walker-type circulation anomaly is formed. Correspondingly, convection and precipitation processes in the Arabian Sea are diminished, resulting in less isotopically depleted water vapor transported westward, and ultimately a higher ID $\delta^{18}O_p$ (Fig. 9c), and vice versa (Fig. 9d).

This study only qualitatively analyzes the effects of convection and moisture transport related to regional monsoon activity on $\delta^{18}O_p$ variations. Yet, our results strongly suggest that the interannual variation of $\delta^{18}O_p$ in different AMRs is associated with the variation in intensity of different monsoon subsystems. However, due to the limited time range of the research data, it remains unclear whether the same mechanisms exist on decadal or longer timescales. In addition, there are many factors influencing the variations of AMR $\delta^{18}O_p$, although this study only focuses on the modulating role of the monsoons. Therefore, it is necessary to further explore the in-depth physical mechanisms and longer time scale relationships between $\delta^{18}O_p$ and the monsoon, which are of crucial importance in reconstructing and understanding the history of changes in the Asian paleomonsoon.

Declaration of Competing Interest

The authors declare no competing interests.

Data availability

The data that support the findings of this study are openly available at the following URL/DOI: the NCEP/DOE reanalysis data: https://psl.noaa.gov/data/gridded/data.ncep.reanalysis2.html.ncep.reanalysis2.html, the CMAP data: https://psl.noaa.gov/data/gridded/data.cmap.html.html, the OLR data: https://psl.noaa.gov/data/gridded/data.olrcdr.interp.html, the isoGSM2 isotope data: https://datadryad.org/stash/dataset/doi:10.6078/D1MM6B (Chiang et al., 2020), the ECHAM6-wiso isotope data: https://doi.org/10.5281/zenodo.5636328.5636328 (Cauquoin and Werner, 2021).

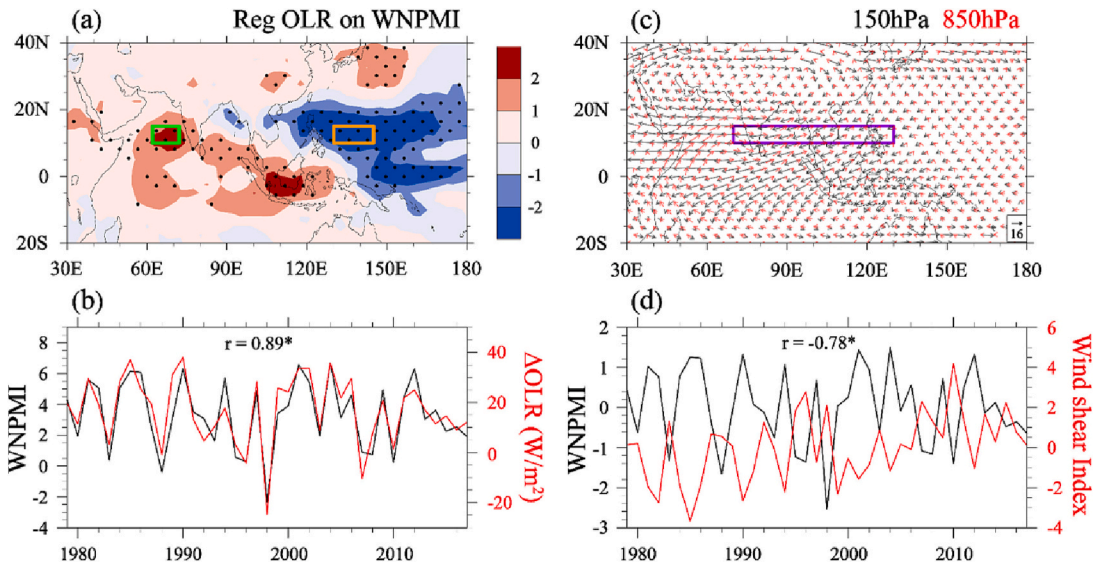

Fig. 8. (a) Regressed summer OLR (W/m^2) against WNPMI during 1979–2017; (b) Time series of the WNPMI and ΔOLR from 1979 to 2017; (c) Climatological summer wind fields (m/s) at 850 hPa and 150 hPa; (d) Same as (b), but for the normalized WNPMI and USI; The "r" represents the correlation coefficient between the two series, and the "*" means exceeding the 99% confidence level.

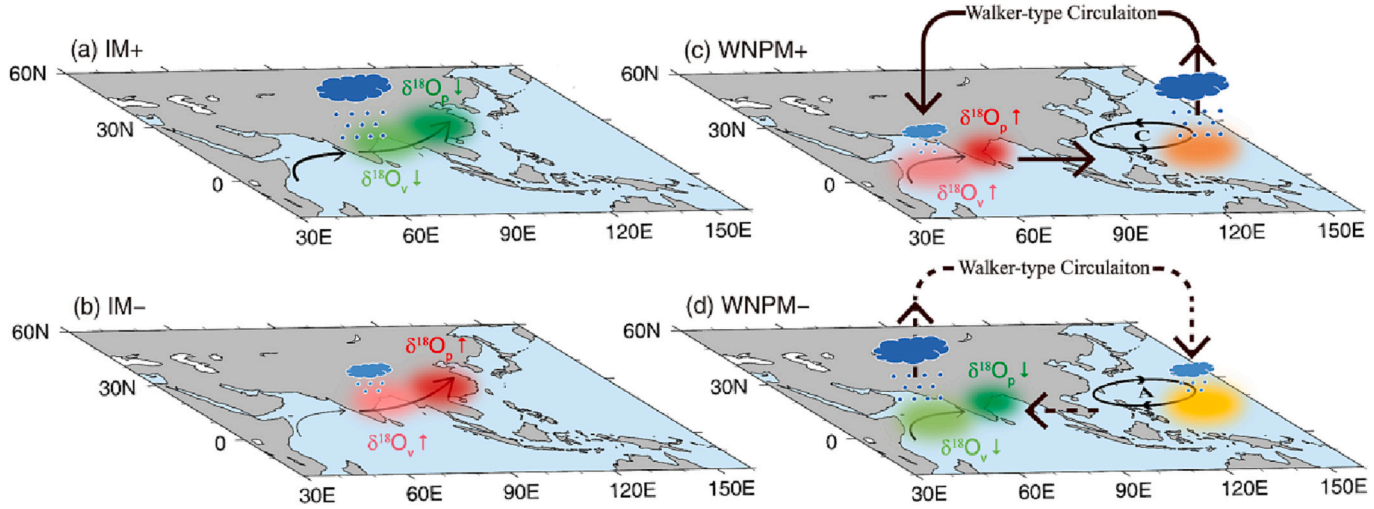

Fig. 9. Schematic diagram of the relationships between spatial patterns of $\delta^{18}O_p$ changes and configurations of atmospheric circulation anomalies under different regional monsoon intensity conditions. (a) Strong IM years; (b)Weak IM years; (c) Strong WNPM years; (d) Weak WNPM years. See the text for details.

Acknowledgments

We thank two anonymous reviewers for their constructive comments and suggestions that have helped us to improve the manuscript. This work was supported by the Fund of Shandong Province (LSKJ202203300); the Strategic Priority Research Program of the Chinese Academy of Sciences (XDB40030100); and the National Natural Science Foundation of China (42105049).

Appendix A. Supplementary data

Supplementary data to this article can be found online at https://doi.org/10.1016/j.gloplacha.2023.104187.

References

Araguás-Araguás, L., Froehlich, K., Rozanski, K., 1998. Stable isotope composition of precipitation over Southeast Asia. J. Geophys. Res. 103, 28721–28742. https://doi.org/10.1029/98jd02582.

Araguás-Araguás, L., Froehlich, K., Rozanski, K., 2000. Deuterium and oxygen-18 isotope composition of precipitation and atmospheric moisture. Hydrol. Process. 14, 1341–1355. https://doi.org/10.1002/1099-1085(20000615)14:8<1341::AID-HYP983>3.0.CO;2-Z.

Bedaso, Z.K., DeLuca, N.M., Levin, N.E., Zaitchik, B.F., Waugh, D.W., Wu, S.Y., Harman, C.J., Shanko, D., 2020. Spatial and temporal variation in the isotopic composition of Ethiopian precipitation. J. Hydrol. 585, 124364 https://doi.org/10.1016/j.jhydrol.2019.124364.

Cai, Z.Y., Tian, L.D., 2016a. Processes governing water vapor isotope composition in the Indo-Pacific region: convection and water vapor transport. J. Clim. 29, 8535–8546. https://doi.org/10.1175/Jcli-D-16-0297.1.

Cai, Z.Y., Tian, L.D., 2016b. Atmospheric controls on seasonal and interannual variations in the precipitation isotope in the East Asian monsoon region. J. Clim. 29, 1339–1352. https://doi.org/10.1175/Jcli-D-15-0363.1.

Castillo, R., Nieto, R., Drumond, A., Gimeno, L., 2014. The role of the ENSO cycle in the modulation of moisture transport from major oceanic moisture sources. Water Resour. Res. 50, 1046–1058. https://doi.org/10.1002/2013wr013900.

Cauquoin, A., Werner, M., 2021. High-resolution nudged isotope modeling with ECHAM6-wiso: impacts of updated model physics and ERA5 reanalysis data. J. Adv. Model. Earth Syst. 13, 1–19. https://doi.org/10.1029/2021ms002532.

Cauquoin, A., Werner, M., Lohmann, G., 2019. Water isotopes – climate relationships for the mid-Holocene and preindustrial period simulated with an isotope-enabled version of MPI-ESM. Clim. Past 15, 1913–1937. https://doi.org/10.5194/cp-15-1913-2019.

Chiang, J.C.H., Herman, M.J., Yoshimura, K., Fung, I.Y., 2020. Enriched East Asian oxygen isotope of precipitation indicates reduced summer seasonality in regional climate and westerlies. Proc. Natl. Acad. Sci. U. S. A. 117, 14745–14750. https://doi.org/10.1073/pnas.1922602117.

Cole, J.E., Rind, D., Webb, R.S., Jouzel, J., Healy, R., 1999. Climatic controls on interannual variability of precipitation $\delta^{18}O$: simulated influence of temperature, precipitation amount, and vapor source region. J. Geophys. Res.-Atmos. 104, 14223–14235. https://doi.org/10.1029/1999jd900182.

Dansgaard, W., 1964. Stable isotopes in precipitation. Tellus 16, 436–468. https://doi.org/10.3402/tellusa.v16i4.8993.

Feng, A.X., Gong, Z.Q., Wang, Q.G., Feng, G.L., 2012. Three-dimensional air–sea interactions investigated with bilayer networks. Theor. Appl. Climatol. 109, 635–643. https://doi.org/10.1007/s00704-012-0600-7.

Gastmans, D., Santos, V., Galhardi, J.A., Gromboni, J.F., Batista, L.V., Miotlinski, K., Chang, H.K., Govone, J.S., 2017. Controls over spatial and seasonal variations on isotopic composition of the precipitation along the central and eastern portion of Brazil. Isot. Environ. Health Stud. 53, 518–538. https://doi.org/10.1080/10256016.2017.1305376.

Gat, J.R., 1996. Oxygen and hydrogen isotopes in the hydrologic cycle. Annu. Rev. Earth Planet. Sci. 24, 225–262. https://doi.org/10.1146/annurev.earth.24.1.225.

Gimeno, L., Stohl, A., Trigo, R.M., Dominguez, F., Yoshimura, K., Yu, L., Drumond, A., Durán-Quesada, A.M., Nieto, R., 2012. Oceanic and terrestrial sources of continental precipitation. Rev. Geophys. 50, RG4003. https://doi.org/10.1029/2012rg000389.

Hastenrath, S., 2000. Zonal circulations over the equatorial Indian Ocean. J. Clim. 13, 2746–2756. https://doi.org/10.1175/1520-0442(2000)013<2746:ZCOTEI>2.0.CO;2.

Hersbach, H., et al., 2020. The ERA5 global reanalysis. Q. J. R. Meteorol. Soc. 146, 1999–2049. https://doi.org/10.1002/qj.3803.

Hoffmann, G., Heimann, M., 1997. Water isotope modeling in the Asian monsoon region. Quat. Int. 37, 115–128. https://doi.org/10.1016/1040-6182(96)00004-3.

Hughes, C.E., Crawford, J., 2013. Spatial and temporal variation in precipitation isotopes in the Sydney Basin, Australia. J. Hydrol. 489, 42–55. https://doi.org/10.1016/j.jhydrol.2013.02.036.

Ishizaki, Y., Yoshimura, K., Kanae, S., Kimoto, M., Kurita, N., Oki, T., 2012. Interannual variability of $H_2^{18}O$ in precipitation over the Asian monsoon region. J. Geophys. Res.-Atmos. 117, 1–16. https://doi.org/10.1029/2011jd015890.

Jia, W.X., Xu, X.T., Yuan, R.F., Ma, X.G., Zhu, G.F., Li, Z.X., 2019. Variation characteristics of stable isotopes in precipitation and the environmental factors that influence them in the Shiyang River Basin of China. China Environ. Earth Sci. 78, 306. https://doi.org/10.1007/s12665-019-8307-z.

Johnson, K.R., Ingram, B.L., 2004. Spatial and temporal variability in the stable isotope systematics of modern precipitation in China: implications for paleoclimate reconstructions. Earth Planet. Sci. Lett. 220, 365–377. https://doi.org/10.1016/s0012-821x(04)00036-6.

Kanamitsu, M., et al., 2002. NCEP–DOE AMIP-II reanalysis (R-2). Bull. Am. Meteorol. Soc. 83, 1631–1644. https://doi.org/10.1175/BAMS-83-11-1631.

Kathayat, G., Sinha, A., Tanoue, M., Yoshimura, K., Li, H.Y., Zhang, H.W., Cheng, H., 2021. Interannual oxygen isotope variability in Indian summer monsoon precipitation reflects changes in moisture sources. Commun. Earth Environ. 2, 1–10. https://doi.org/10.1038/s43247-021-00165-z.

Lau, N.C., Nath, M.J., 2003. Atmosphere–Ocean variations in the Indo-Pacific sector during ENSO episodes. J. Clim. 16, 3–20. https://doi.org/10.1175/1520-0442(2003)016<0003:AOVITI>2.0.CO;2.

Li, R.C.Y., Zhou, W., 2014. Interdecadal change in South China Sea tropical cyclone frequency in association with zonal sea surface temperature gradient. J. Clim. 27, 5468–5480. https://doi.org/10.1175/jcli-d-13-00744.1.

Lee, J.E., Risi, C., Fung, I., Worden, J., Scheepmaker, R.A., Lintner, B., Frankenberg, C., 2012. Asian monsoon hydrometeorology from TES and SCIAMACHY water vapor isotope measurements and LMDZ simulations: Implications for speleothem climate record interpretation. J. Geophys. Res.-Atmos. 117, D15112. https://doi.org/10.1029/2011JD017133.

Li, J.M., Ehlers, T.A., Mutz, S.G., Steger, C., Paeth, H., Werner, M., Poulsen, C.J., Feng, R., 2016. Modern precipitation $\delta^{18}O$ and trajectory analysis over the Himalaya-Tibet Orogen from ECHAM5-wiso simulations. J. Geophys. Res.-Atmos. 121, 10432–10452. https://doi.org/10.1002/2016jd024818.

Liebmann, B., Smith, C.A., 1996. Description of a complete (interpolated) outgoing longwave radiation dataset. Bull. Am. Meteorol. Soc. 77, 1275–1277.

Liu, J.R., Song, X.F., Yuan, G.F., Sun, X.M., Liu, X., Wang, Z.M., Wang, S.Q., 2008. Stable isotopes of summer monsoonal precipitation in southern China and the moisture sources evidence from $\delta^{18}O$ signature. J. Geogr. Sci. 18, 155–165. https://doi.org/10.1007/s11442-008-0155-9.

Liu, X.D., Xie, X.X., Guo, Z.T., Yin, Z.Y., Chen, G.S., 2022. Model-based orbital-scale precipitation $\delta^{18}O$ variations and distinct mechanisms in Asian monsoon and arid regions. Natl. Sci. Rev. 9, https://doi.org/10.1093/nsr/nwac182 nwac182.

Midhun, M., Ramesh, R., 2016. Validation of $\delta^{18}O$ as a proxy for past monsoon rain by multi-GCM simulations. Clim. Dyn. 46, 1371–1385. https://doi.org/10.1007/s00382-015-2652-8.

Midhun, M., Lekshmy, P.R., Ramesh, R., Yoshimura, K., Sandeep, K.K., Kumar, S., Sinha, R., Singh, A., Srivastava, S., 2018. The effect of monsoon circulation on the stable isotopic composition of rainfall. J. Geophys. Res.-Atmos. 123, 5205–5221. https://doi.org/10.1029/2017jd027427.

Murakami, T., Matsumoto, J., 1994. Summer monsoon over the Asian continent and Western North Pacific. J. Meteorol. Soc. Jpn. 72, 719–745. https://doi.org/10.2151/jmsj1965.72.5_719.

Pathak, A., Ghosh, S., Martinez, J.A., Dominguez, F., Kumar, P., 2017. Role of Oceanic and land moisture sources and transport in the seasonal and interannual variability of summer monsoon in India. J. Clim. 30, 1839–1859. https://doi.org/10.1175/jcli-d-16-0156.1.

Pausata, F.S.R., Battisti, D.S., Nisancioglu, K.H., Bitz, C.M., 2011. Chinese stalagmite $\delta^{18}O$ controlled by changes in the Indian monsoon during a simulated Heinrich event. Nat. Geosci. 4, 474–480. https://doi.org/10.1038/ngeo1169.

Pohl, B., Camberlin, P., 2011. Intraseasonal and interannual zonal circulations over the Equatorial Indian Ocean. Theor. Appl. Climatol. 104, 175–191. https://doi.org/10.1007/s00704-010-0336-1.

Posmentier, E.S., Feng, X.H., Zhao, M.X., 2004. Seasonal variations of precipitation $\delta^{18}O$ in eastern Asia. J. Geophys. Res. 109, D23106. https://doi.org/10.1029/2004jd004510.

Prasad, K.D., Bansod, S.D., 2000. Interannual variations of outgoing longwave radiation and Indian summer monsoon rainfall. Int. J. Climatol. 20, 1955–1964. https://doi.org/10.1002/1097-0088(200012)20:15<1955::AID-JOC589>3.3.CO;2-N.

Rahul, P., Ghosh, P., 2019. Long term observations on stable isotope ratios in rainwater samples from twin stations over Southern India; identifying the role of amount effect, moisture source and rainout during the dual monsoons. Clim. Dyn. 52, 6893–6907. https://doi.org/10.1007/s00382-018-4552-1.

Risi, C., Bony, S., Vimeux, F., Jouzel, J., 2010. Water-stable isotopes in the LMDZ4 general circulation model: model evaluation for present-day and past climates and applications to climatic interpretations of tropical isotopic records. J. Geophys. Res.-Atmos. 115, D013255. https://doi.org/10.1029/2009jd013255.

Rozanski, K., Araguás-Araguás, L., Gonfiantini, R., 1993. Isotopic patterns in modern global precipitation. In: Swart, P.K., Lohmann, K.C., McKenzie, J., Savin, S. (Eds.), Climate Change in Continental Isotopic Records. American Geophysical Union, Washington, pp. 1–36.

Ruan, J.Y., Zhang, H.Y., Cai, Z.Y., Yang, X.Q., Yin, J., 2019. Regional controls on daily to interannual variations of precipitation isotope ratios in Southeast China: implications for paleomonsoon reconstruction. Earth Planet. Sci. Lett. 527, 115794 https://doi.org/10.1016/j.epsl.2019.115794.

Salamalikis, V., Argiriou, A.A., Dotsika, E., 2016. Isotopic modeling of the sub-cloud evaporation effect in precipitation. Sci. Total Environ. 544, 1059–1072. https://doi.org/10.1016/j.scitotenv.2015.11.072.

Sheng, C., He, B., Wu, G.X., Liu, Y.M., Zhang, S.Y., Zhang, P., 2022. Interannual impact of the North Atlantic tripole SST mode on the surface potential vorticity over the Tibetan Plateau during Boreal summer. J. Geophys. Res.-Atmos. 127, 1–17. https://doi.org/10.1029/2021jd036369.

Stevens, B., et al., 2013. Atmospheric component of the MPI-M Earth system model: ECHAM6. J. Adv. Model. Earth Syst. 5, 146–172. https://doi.org/10.1002/jame.20015.

Sutanto, S.J., Hoffmann, G., Worden, J., Scheepmaker, R.A., Aben, I., Röckmann, T., 2015. Atmospheric processes governing the changes in water isotopologues during ENSO events from model and satellite measurements. J. Geophys. Res.-Atmos. 120, 6712–6729. https://doi.org/10.1002/2015jd023228.

Tan, M., 2014. Circulation effect: response of precipitation $\delta^{18}O$ to the ENSO cycle in monsoon regions of China. Clim. Dyn. 42, 1067–1077. https://doi.org/10.1007/s00382-013-1732-x.

Tang, Y., Song, X.F., Zhang, Y.H., Han, D.M., Ai, L.K., Zhao, T.B., Wang, Y.J., 2017. Using stable isotopes to understand seasonal and interannual dynamics in moisture sources and atmospheric circulation in precipitation. Hydrol. Process. 31, 4682–4692. https://doi.org/10.1002/hyp.11388.

Terray, P., Delecluse, P., Labattu, S., Terray, L., 2003. Sea surface temperature associations with the late Indian summer monsoon. Clim. Dyn. 21, 593–618. https://doi.org/10.1007/s00382-003-0354-0.

Tian, Y., Zhang, H.W., Zhang, R., Zhang, F., Liang, Z.Y., Cai, Y.J., Cheng, H., 2021. Seasonal and inter-annual variations of stable isotopic characteristics of rainfall and cave water in Shennong cave, Southeast China, and its paleoclimatic implication. Front. Earth Sci. 9, 794762 https://doi.org/10.3389/feart.2021.794762.

Vuille, M., Werner, M., Bradley, R.S., Keimig, F., 2005. Stable isotopes in precipitation in the Asian monsoon region. J. Geophys. Res.-Atmos. 110, D23108. https://doi.org/10.1029/2005jd006022.

Wang, B., LinHo, 2002. Rainy season of the Asian–Pacific summer monsoon. J. Clim. 15, 386–398. https://doi.org/10.1175/1520-0442(2002)015<0386:RSOTAP>2.0.CO;2.

Wang, B., Xu, X.H., 1997. Northern hemisphere summer monsoon singularities and climatological intraseasonal oscillation. J. Clim. 10, 1071–1085. https://doi.org/10.1175/1520-0442(1997)010<1071:NHSMSA>2.0.CO;2.

Wang, B., Wu, R.G., Lau, K.M., 2001. Interannual variability of the Asian summer monsoon: contrasts between the Indian and the Western North Pacific–East Asian monsoons. J. Clim. 14, 4073–4090. https://doi.org/10.1175/1520-0442(2001)014<4073:IVOTAS>2.0.CO;2.

Wang, B., Wu, Z.W., Li, J.P., Liu, J., Chang, C.P., Ding, Y.H., Wu, G.X., 2008. How to measure the strength of the East Asian summer monsoon. J. Clim. 21, 4449–4463. https://doi.org/10.1175/2008jcli2183.1.

Wang, B., Xiang, B., Lee, J.Y., 2013. Subtropical high predictability establishes a promising way for monsoon and tropical storm predictions. Proc. Natl. Acad. Sci. U. S. A. 110, 2718–2722. https://doi.org/10.1073/pnas.1214626110.

Wang, S.J., Zhang, M.J., Hughes, C.E., Zhu, X.F., Dong, L., Ren, Z.G., Chen, F.L., 2016. Factors controlling stable isotope composition of precipitation in arid conditions: an observation network in the Tianshan Mountains, Central Asia. Tellus Ser. B Chem. Phys. Meteorol. 68, 26206. https://doi.org/10.3402/tellusb.v68.26206.

Wang, Y.Z., Hu, C.Y., Ruan, J.Y., Johnson, K.R., 2020. East Asian precipitation $\delta^{18}O$ relationship with various monsoon indices. J. Geophys. Res.-Atmos. 125, https://doi.org/10.1029/2019jd032282 e2019JD032282.

Wang, Y.M., Wu, B., Zhou, T.J., 2022. Maintenance of Western North Pacific anomalous anticyclone in Boreal summer by wind-induced moist enthalpy advection mechanism. J. Clim. 35, 4499–4511. https://doi.org/10.1175/jcli-d-21-0708.1.

Webster, P.J., 1994. The role of hydrological processes in ocean-atmosphere interactions. Rev. Geophys. 32, 427–476. https://doi.org/10.1029/94RG01873.

Webster, P.J., Yang, S., 1992. Monsoon and Enso: selectively interactive systems. Q. J. R. Meteorol. Soc. 118, 877–926. https://doi.org/10.1002/qj.49711850705.

Werner, M., Langebroek, P.M., Carlsen, T., Herold, M., Lohmann, G., 2011. Stable water isotopes in the ECHAM5 general circulation model: toward high-resolution isotope modeling on a global scale. J. Geophys. Res. Atmos. 116, D15109. https://doi.org/10.1029/2011jd015681.

Wilks, D.S., 2019. Statistical Methods in the Atmospheric Sciences, forth ed. Elsevier, Amsterdam.

Wu, B., Zhou, T.J., Li, T., 2009. Seasonally evolving dominant interannual variability modes of East Asian climate*. J. Clim. 22, 2992–3005. https://doi.org/10.1175/2008jcli2710.1.

Xie, P.P., Arkin, P.A., 1997. Global precipitation: a 17-year monthly analysis based on gauge observations, satellite estimates, and numerical model outputs. Bull. Am. Meteorol. Soc. 78, 2539–2558. https://doi.org/10.1175/1520-0477(1997)078<2539:GPAYMA>2.0.CO;2.

Yang, X.X., Yao, T.D., Yang, W.L., Xu, B.Q., He, Y., Qu, D.M., 2012. Isotopic signal of earlier summer monsoon onset in the Bay of Bengal. J. Clim. 25, 2509–2516. https://doi.org/10.1175/jcli-d-11-00180.1.

Yang, H., Johnson, K.R., Griffiths, M.L., Yoshimura, K., 2016. Interannual controls on oxygen isotope variability in Asian monsoon precipitation and implications for paleoclimate reconstructions. J. Geophys. Res. Atmos. 121, 8410–8428. https://doi.org/10.1002/2015jd024683.

Yang, S., Zhang, M.J., Wang, S.J., Liu, Y.M., Qiang, F., Qu, D.Y., 2017. Interannual trends in stable oxygen isotope composition in precipitation of China during 1979–2007: spatial incoherence. Quat. Int. 454, 25–37. https://doi.org/10.1016/j.quaint.2017.07.029.

Yim, S.Y., Yeh, S.W., Wu, R.G., Jhun, J.G., 2008. The influence of ENSO on decadal variations in the relationship between the East Asian and Western North Pacific summer monsoons. J. Clim. 21, 3165–3179. https://doi.org/10.1175/2007jcli1948.1.

Yoshimura, K., Kanamitsu, M., Noone, D., Oki, T., 2008. Historical isotope simulation using reanalysis atmospheric data. J. Geophys. Res. 113, D19108. https://doi.org/10.1029/2008jd010074.

Yu, W.S., Wei, F.L., Ma, Y.M., Liu, W.J., Zhang, Y.Y., Luo, L., Tian, L.D., Xu, B.Q., Qu, D. M., 2016. Stable isotope variations in precipitation over Deqin on the southeastern margin of the Tibetan Plateau during different seasons related to various meteorological factors and moisture sources. Atmos. Res. 170, 123–130. https://doi.org/10.1016/j.atmosres.2015.11.013.

Zhou, J.L., Li, T.Y., 2018. A tentative study of the relationship between annual $\delta^{18}O$ & δD variations of precipitation and atmospheric circulations—a case from Southwest China. Quat. Int. 479, 117–127. https://doi.org/10.1016/j.quaint.2017.05.038.

Zhou, H., Zhang, X.P., Yao, T.C., Hua, M.Q., Wang, X.J., Rao, Z.G., He, X.G., 2019. Variation of $\delta^{18}O$ in precipitation and its response to upstream atmospheric convection and rainout: a case study of Changsha station, south-Central China. Sci. Total Environ. 659, 1199–1208. https://doi.org/10.1016/j.scitotenv.2018.12.396.